ERTEL POTENTIAL VORTICITY, BERNOULLI STREAMFUNCTION, PLANETARY-SCALE HYDRAULIC JUMPS, AND TRANSONIC JET-STREAKS IN A RE-ANALYSIS OF THE MARTIAN ATMOSPHERE

Stephen R. Lewis, *School of Physical Sciences, The Open University, Walton Hall, Milton Keynes MK7 6AA, UK (stephen.lewis@open.ac.uk),* **Timothy E. Dowling,** *Department of Physics & Astronomy, University of Louisville, Kentucky 40292, USA,* **Mary Elizabeth Bradley,** *Department of Mathematics, University of Louisville, Kentucky 40292, USA,* **Peter L. Read,** *Atmospheric, Oceanic and Planetary Physics, University of Oxford OX1 3PU, UK.*

Introduction:

An analysis of the martian global atmospheric state, on potential temperature (isentropic) surfaces, shows a functional relationship between Ertel potential vorticity, *Q*, and Bernoulli streamfunction, *B*. The strength of the relationship obtained indicates that nonlinear advection of potential vorticity is weak in the martian atmosphere even though gradients are strong. Two features of this analysis stand out: (i) a planetary-scale ring of hydraulic jumps can be inferred where the Froude number, *Fr*, transitions between streaming (*Fr* < 1) and shooting (*Fr* > 1) flow on the poleward flank of the polar jet (Dowling et al. 2016a), and ii) jet streaks that reach sonic speed with Mach number, *Ma* = 1.0 (Dowling et al. 2016b). Froude-number and Mach-number calculations are commonly used in aeronautics and the engineering thermal-fluid sciences, but are much less frequently employed for Earth-based meteorological applications. Mars might be different in this regard and we discuss some of the implications, further work with models using data assimilation techniques, and how these quantities might be measured in practice.

Method:

For the analysis shown, we primarily use the Mars Analysis Correction Data Assimilation (MACDA) dataset, version 1.0 (Montabone et al. 2014), which is openly available via the British Atmospheric Data Centre (BADC). This reanalysis was created by assimilating nadir soundings from the NASA Mars Global Surveyor (MGS) Thermal Emission Spectrometer (TES) into the United Kingdom (UK) version of the Laboratoire de Météorologie Dynamique (LMD) Mars Global Circulation Model (MGCM), developed through a collaboration between groups in France (Forget et al. 1999), the UK (Lewis et al. 1999) and Spain (González-Galindo et al. 2009).

Data from MACDA were interpolated, using cubic splines, to isentropic surfaces (see Fig. 1) making use of the Explicit Planetary Isentropic Coordinate (EPIC) atmospheric model (Dowling et al. 1998, 2006), where further analysis was performed on potential temperature, θ surfaces. Ertel potential vorticity,

$$Q = \frac{\zeta + f}{h},$$

where ζ is the relative vorticity, *f* is the planetary vorticity and

$$h = -\frac{1}{g}\frac{\partial \theta}{\partial p},$$

and Bernoulli streamfunction,

$$B = \phi + c_p T + K,$$

where ϕ is the geopotential, $c_p T$ is the specific enthalpy and *K* is the specific horizontal kinetic energy, were both calculated at every point on each θ surface.

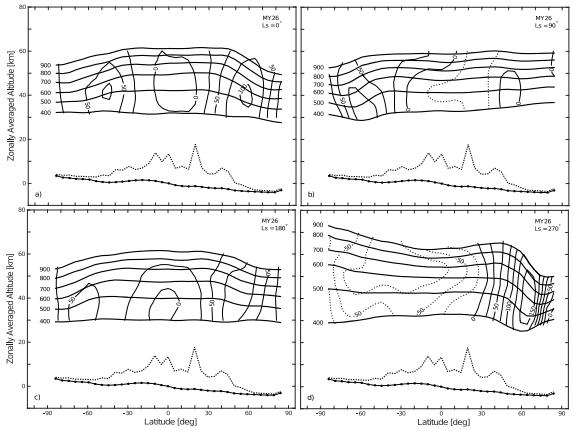

Figure 1: Analysis surfaces in the four canonical seasons for Mars Year (MY) 26 as a function of altitude. The thick, horizontally orientated curves show isentropic surfaces, labelled by potential temperature, from θ = 400 to 900 K (~30 to 60 km). The thin contours show the zonally averaged zonal (east-west) wind, in increments of 25 ms^{-1}. The dotted curve at the bottom is the silhouette of the highest topography; the associated smooth curve is the zonal average of the topography, marked by black dots to indicate the 5° resolution of the MACDA data set. Reproduced from Dowling et al. (2016a).

Correlations between *Q* and *B*, on each θ surface and at each time, were examined and a simple, linear model was fitted, with a correlation coefficient $\mu_0(\theta, t)$, using the form

$$\frac{Q}{Q_0} = 1 - \mu_0(B - B_0).$$

Further analyses were conducted by finding the pointwise Froude number

$$Fr = \sqrt{\frac{2K}{(NH)^2}},$$

where N is the buoyancy frequency and H the pressure scale height. The Froude number is the ratio of wind speed to gravity wave speed. The analogous quantity for sound waves is the Mach number,

$$Ma = \frac{\sqrt{2K}}{c_{\text{sound}}}$$

where c_{sound} for carbon dioxide gas varies from about 190–240 m s^{-1} over the typical temperature range T=130–220 K that is encountered on Mars at these altitudes.

Results:

In both hemispheres, in autumn, winter and spring, the correlation between Q and B is positive, but decreases slowly with height. The correlation is close to zero in the southern hemisphere summer and in northern hemisphere summer, the correlation can become negative. This behaviour is reminiscent of the Earth's lower mesosphere (roughly z=48–62 km). One striking difference between the planets is that Mars exhibits a large range of Q poleward of each winter polar jet and a strong annular vortex structure.

Figure 2 shows the scatter of points and linear model fit in the northern hemisphere at four cardinal times of year on Mars and on three of the θ-surfaces. Figure 3 shows an expanded view of the winter hemisphere scatter in both the northern and southern hemispheres. At this time of year there is a very characteristic, shoe-like shape with points to the right (toe) typically from tropical regions, points across the centre (arch) from mid-latitudes and the main westerly jet around the pole and points to the lower left (heel) originating from the poleward side of the jet and over the winter pole. Between each winter polar jet and pole, especially in the north, there is a large spread of Q over a small domain of B, which is unlike Earth and may be related to one or more hydraulic jumps in the region as air can move between shooting and streaming with deformation and curvature in the poleward edge of the jet. The Froude number reveals that the points poleward of the jet are streaming (Fr < 1), whereas jet points are often shooting (Fr > 1) or strongly shooting (Fr > 2), shown by circles in Fig. 3.

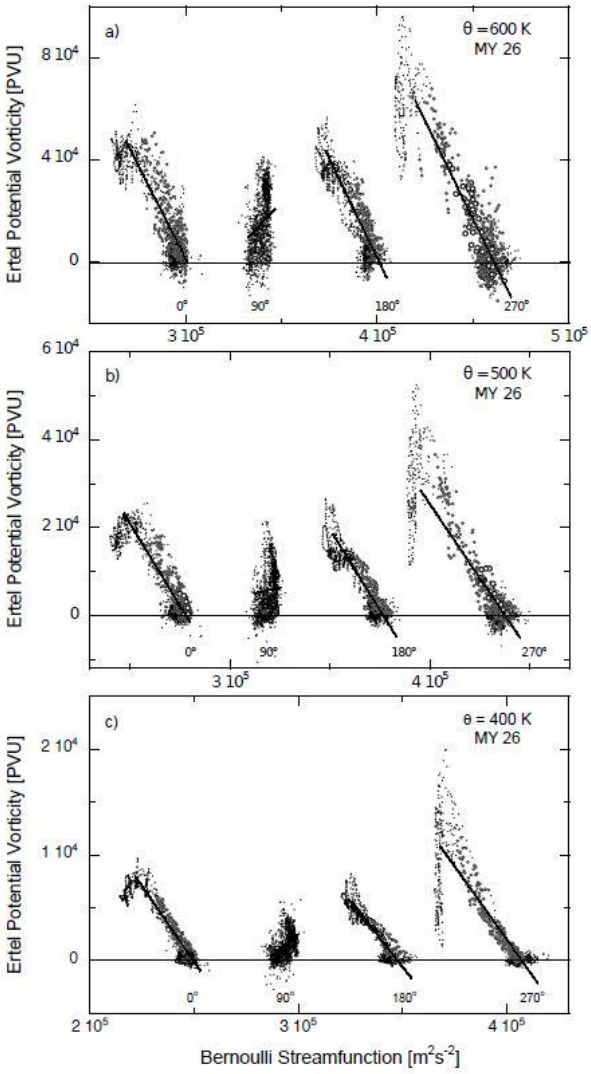

Figure 2: Scatter plots of Ertel potential vorticity versus Bernoulli streamfunction in the martian northern hemisphere with lines showing the linear *Q(B)* model for snapshots at the four canonical season points in MY 26, on potential-temperature levels a) θ = 600 K, b) 500K and c) 400 K. B is shifted by 0.5 × 10^5 m^{2}s^{-2} between seasons for clarity. The regression is performed on the data falling in the range 30–70° N, but the scatter shows all points in the hemisphere, including the tropical region points which tend to lie to the right, lower end of each cluster. Reproduced from Dowling et al. (2016a).

In the centre of the northern hemisphere winter jet, at 60–70° N, and in the region θ = 500–600 K (roughly 35–40 km altitude, see Fig. 1d), the martian winter is transonic with 0.8 < Ma < 1.2.

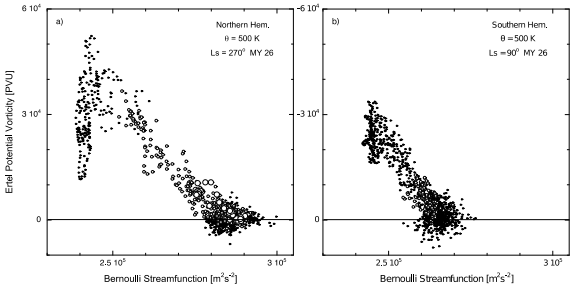

Figure 3: Scatter plots of Ertel potential vorticity versus Bernoulli streamfunction on potential temperature surface θ = 500 K, for the Martian a) northern winter, L_s = 270° and b) southern winter, L_s = 90°, both in MY 26. Points are labelled by Froude number, *Fr*, with the small-black dots, small-open circles and large-open circles corresponding to $0 \leq Fr < 1$ (streaming), $1 \leq Fr < 2$ (shooting) and $2 \leq Fr$ (strongly shooting) flow, respectively (the latter only occur here in panel a). Reproduced from Dowling et al. (2016a).

Figure 4 shows how the correlation, $\mu_0(\theta = 550\ \mathrm{K}, t)Q_0$, varies over two MY (25 and 26) of the MACDA re-analysis. Significant and rapid variations in the correlation parameter, and in the static stability of the atmosphere, are either linked to periods of data loss, when the assimilation tends to return to a model-only solution (Lewis et al. 2007), or to major dust storm events, such as the global storm in MY25 and a significant regional dust storm in MY26 (Kass et al. 2016).

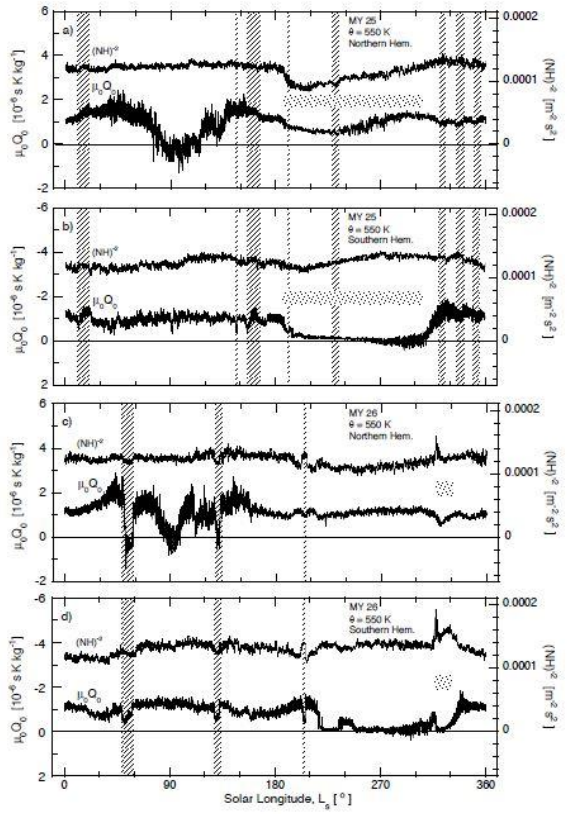

Figure 4: Time series of the correlation parameter, $\mu_0 Q_0$, and $\left[\ \overline{(NH)^2}\ \right]^{-1}$ on θ = 550 K for MY 25 in the a) northern and b) southern hemisphere, and for MY 26 in the c) northern and d) southern hemisphere. The time span of the MY 25 planet-encircling dust storm (L_S = 185–304°) is indicated by the horizontal stippled band in a) and b), and the time span of a significant regional dust storm in MY 26 (L_S = 316–331°) is likewise indicated in c) and d). Four data points per sol are plotted; vertical hatching indicates the absence of TES observations. The $\mu_0 Q_0$ profiles are plotted as pairs of curves to indicate plus or minus the standard error, with the corresponding (left) ordinate reversed for the southern hemisphere to facilitate comparison between the hemispheres. Reproduced from Dowling et al. (2016a).

Discussion:

These results demonstrate the value of a potential vorticity analysis for Mars, a diagnostic that is not frequently addressed (Barnes and Haberle 1996) owing to the highly diabatic nature of the atmosphere. The strong correlation seen between *Q* and *B* implies only very weak nonlinear advection of *Q* by the horizontal flow, but this state does not imply weak *Q* gradients. The winter polar jet, in particular in the northern hemisphere where it is strongest, exhibits large variations in *Q*. A Froude-number and Mach-number analysis reveals features not reported on Earth: i) transonic jet streaks and ii) the juxtaposition of regions of shooting and streaming flow, which suggests a planetary- scale hydraulic jump.

We are currently examining 3D lagrangian fluid trajectories to better characterize the rotating hydraulics of the system as a function of season. An intriguing possibility in the near future is the use of a similar correlation between potential vorticity and ozone (or other trace gas measurements) in polar regions (Holmes et al. 2016, 2017) to infer the *Q* distribution from measurements to be made by ExoMars Trace Gas Orbiter.

Acknowledgements:

The authors thank Robert Haberle, Luca Montabone, Raymond Pierrehumbert and Andrew White for useful discussions. SRL acknowledges support from STFC grant ST/L000776/1, UKSA grant ST/M00306X/1, the EU Horizon 2020 project UPWARDS ref. 633127 and ESA (MarMITE, ESA contract no. 4000114138/115/NL/PA) for support in related areas. PLR acknowledges STFC grant ST/I0001948/1 and ESA (MarMITE, details above).

References:

Barnes, J. R., and R. M. Haberle (1996), The Martian Zonal-Mean Circulation: Angular Momentum and Potential Vorticity Structure in GCM Simulations, Journal of the Atmospheric Sciences, 53(21), 3143–3156, doi:10.1175/1520-0469(1996)053<3143:TMZMCA>2.0.CO;2.

Dowling, T. E. et al. (2006), The EPIC atmospheric model with an isentropic/terrain-following hybrid vertical coordinate, Icarus, 182(1), 259–273.

Dowling, T. E., M. E. Bradley, J. Du, S. R. Lewis, and P. L. Read (2016a), Ertel potential vorticity versus Bernoulli streamfunction on Mars, Quarterly Journal of the Royal Meteorological Society, doi:10.1002/qj.2916.

Dowling, T. E., M. E. Bradley, S. R. Lewis, and P. L. Read (2016b), Planetary-scale hydraulic jumps and transonic jet-streaks in the MACDA reanalysis of the Martian atmosphere: a comparison with Earth's lower mesosphere, Abstract 210.05, 48th Meeting of the DPS/AAS, Pasadena, CA.

Dowling, T. E., A. S. Fischer, P. J. Gierasch, J. Harrington, R. P. LeBeau, and C. M. Santori (1998), The explicit planetary isentropic-coordinate (EPIC) atmospheric model, Icarus, 132(2), 221–238.

Forget, F., F. Hourdin, R. Fournier, C. Hourdin, O. Talagrand, M. Collins, S. R. Lewis, P. L. Read, and J.-P. Huot (1999), Improved general circulation models of the Martian atmosphere from the surface to above 80 km, Journal of Geophysical Research E: Planets, 104(E10), 24155–24175.

Gonzalez-Galindo, F., F. Forget, M. A. Lopez-Valverde, M. A. I. Coll, and E. Millour (2009), A ground-to-exosphere Martian general circulation model: 1. Seasonal, diurnal, and solar cycle variation of thermospheric temperatures, J Geophys Res-Planet, 114, doi:10.1029/2008JE003246.

Holmes, J. A., S. R. Lewis, and M. R. Patel (2016), On the link between martian total ozone and potential vorticity, Icarus, in press.

Holmes, J. A., S. R. Lewis, and M. R. Patel (2017), On the link between martian total ozone and potential vorticity, this meeting.

Kass, D. M., A. Kleinböhl, D. J. McCleese, J. T. Schofield, and M. D. Smith (2016), Interannual similarity in the Martian atmosphere during the dust storm season, Geophysical Research Letters, 43(12), 6111–6118, doi:10.1002/2016GL068978.

Lewis, S. R., M. Collins, P. L. Read, F. Forget, F. Hourdin, R. Fournier, C. Hourdin, O. Talagrand, and J.-P. Huot (1999), A climate database for Mars, Journal of Geophysical Research E: Planets, 104(E10), 24177–24194.

Lewis, S. R., P. L. Read, B. J. Conrath, J. C. Pearl, and M. D. Smith (2007), Assimilation of thermal emission spectrometer atmospheric data during the Mars Global Surveyor aerobraking period, Icarus, 192(2), 327–347, doi:10.1016/j.icarus.2007.08.009.

Montabone, L., K. Marsh, S. R. Lewis, P. L. Read, M. D. Smith, J. Holmes, A. Spiga, D. Lowe, and A. Pamment (2014), The Mars Analysis Correction Data Assimilation (MACDA) Dataset V1.0, Geosciences Data Journal, 1(2), 129–139, doi:10.1002/gdj3.13.